Solution-Coating Technology for AMOLED Displays

A new solution-coated AMOLED technology is poised for large-format commercial adoption. Improvements in intra- and inter-pixel layer uniformity have driven solution-coated AMOLED displays to match or exceed commercial evaporated AMOLED displays and AMLCDs for short-range uniformity.

by Reid Chesterfield, Andrew Johnson, Charlie Lang, Matthew Stainer, and Jonathan Ziebarth

SOLUTION-BASED coating methods for electronic-device applications are the focus of intense research efforts for many compelling reasons: reduced costs, improved performance, and new functionality, just to name a few. The breadth of applications for passive- and active-element solution-based coatings spans displays, lighting, solar cells, sensors, wireless devices for radio-frequency identification (RFID), and medical devices.[1] Here, the term active refers to using the semiconducting nature of the material as its primary function in a device; for example, in diodes and transistors. Most solution-based coating products that have achieved large-volume manufacturing are confined to passive elements where the electrical conductivity and/or optical or mechanical property of the solution-coated layer are the key to their functionality. Some examples are patterned bus lines, anti-reflective films, planarization layers, and phosphor

Reid Chesterfield is Printing Development Manager at DuPont Displays in Santa Barbara, California. He can be reached at Reid.J.Chesterfield@usa.dupont.com. Andrew Johnson is a Sr. Test Engineer, Charlie Lang is a Technical Fellow, Matthew Stainer is a Principal Investigator, and Jon Ziebarth is a Sr. Research Investigator at DuPont Displays.

layers. Few examples of solution-coated active devices have achieved large-scale commercial production.

Active-matrix organic light-emitting diode (AMOLED) displays are a promising technology in which organic materials are employed to form key active electronic layers. Existing commercial technology for AMOLED displays currently uses thermal evaporation and fine-metal masks to deposit small-molecule materials, but has well-known difficulties in scaling to larger-sized glass.[2] Solution-coating offers the potential for significant cost savings in AMOLED production by reducing material waste and by coating on large-sized glass and may even push AMOLED technology to a cost lower than that for AMLCD technology. A detailed cost model predicts that solution-coated AMOLEDs could cost about 20% less than AMLCDs for small-sized displays,[3] with the savings growing for larger production lines and display sizes such as those for AMOLED TVs.
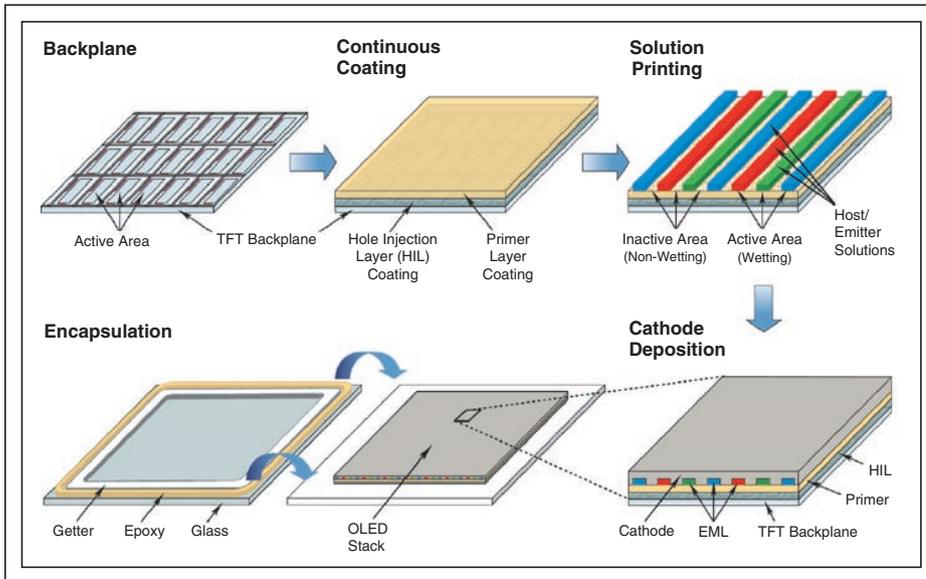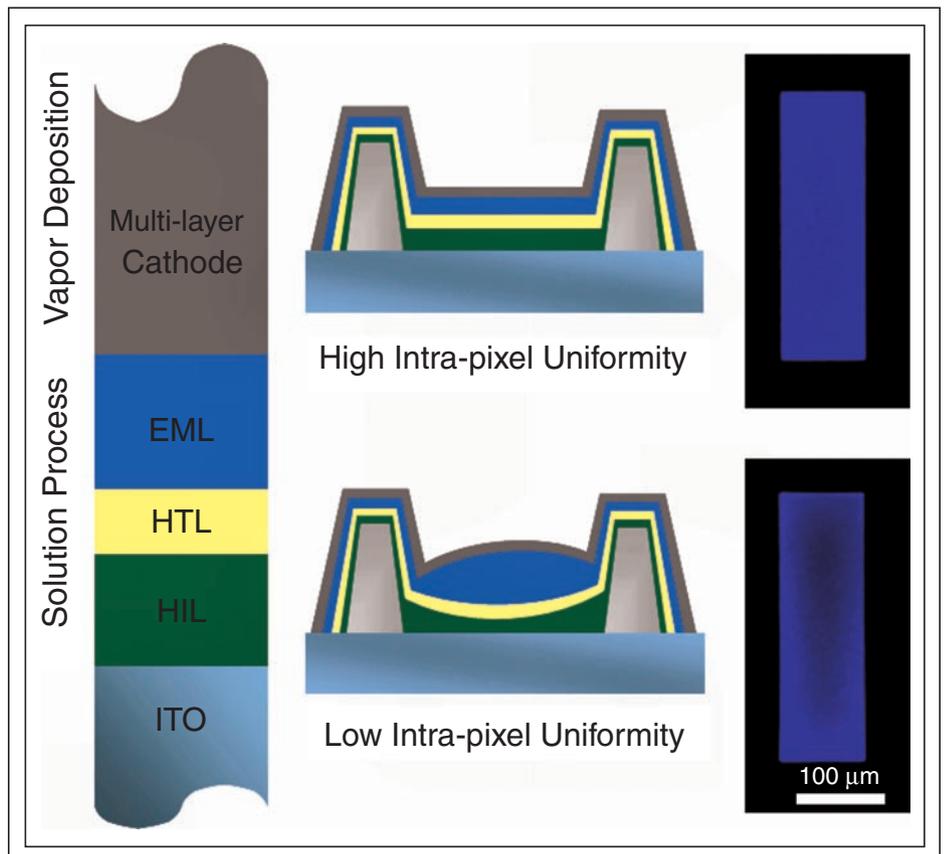
Solution Technology

DuPont Displays has developed a low-cost AMOLED technology that combines high-performance OLED materials tuned for solution-processing, coating techniques, and methods optimized for OLED layers and the

utilization of existing flat-panel-display equipment. This OLED fabrication process is outlined in Fig. 1, in which two solution-coating methods are utilized: slot-coating for blanket layers and continuous nozzle printing for patterned layers. Figure 2 shows a vertical cross-section of an OLED device stack. The hole-injection layer (HIL) and hole-transport layer (HTL) are slot coated; the emissive red, green, and blue layers (EML) are nozzle-printed simultaneously, and a multi-layered cathode is blanket-evaporated. The brightness and color-uniformity specifications for flat-panel displays impose challenging thickness uniformity requirements for solution-coated OLED layers. The uniformity requirements are broken into several areas: long range (across the entire panel), short range (between neighboring pixels or inter-pixel), and within a subpixel (intra-pixel).

Figure 2 shows a schematic cross-section of high and low intra-pixel thickness uniformity and a corresponding example of a blue sub-pixel electroluminescent (EL) image. Inter- and intra-pixel thickness non-uniformity in the solution-coated layers can result in visual defects (mura) as well as non-optimal OLED device performance, and so our technical team developed several new analytical, metrology, and modeling methods to study and improve solution-coated layer uniformity.

Fig. 1: Solution-coated OLED fabrication can be achieved using the above process flow.

85% *vs.* 65% for the spin-coated film. Generally, aperture percentage increases with increasing layer thickness and pixel dimension and apertures above 95% are achievable for larger pixels suitable for AMOLED TV. A previous report from DuPont (cited below) describes the slot-coating process and formulation strategy to optimize coating and drying performance in OLEDs.[5]
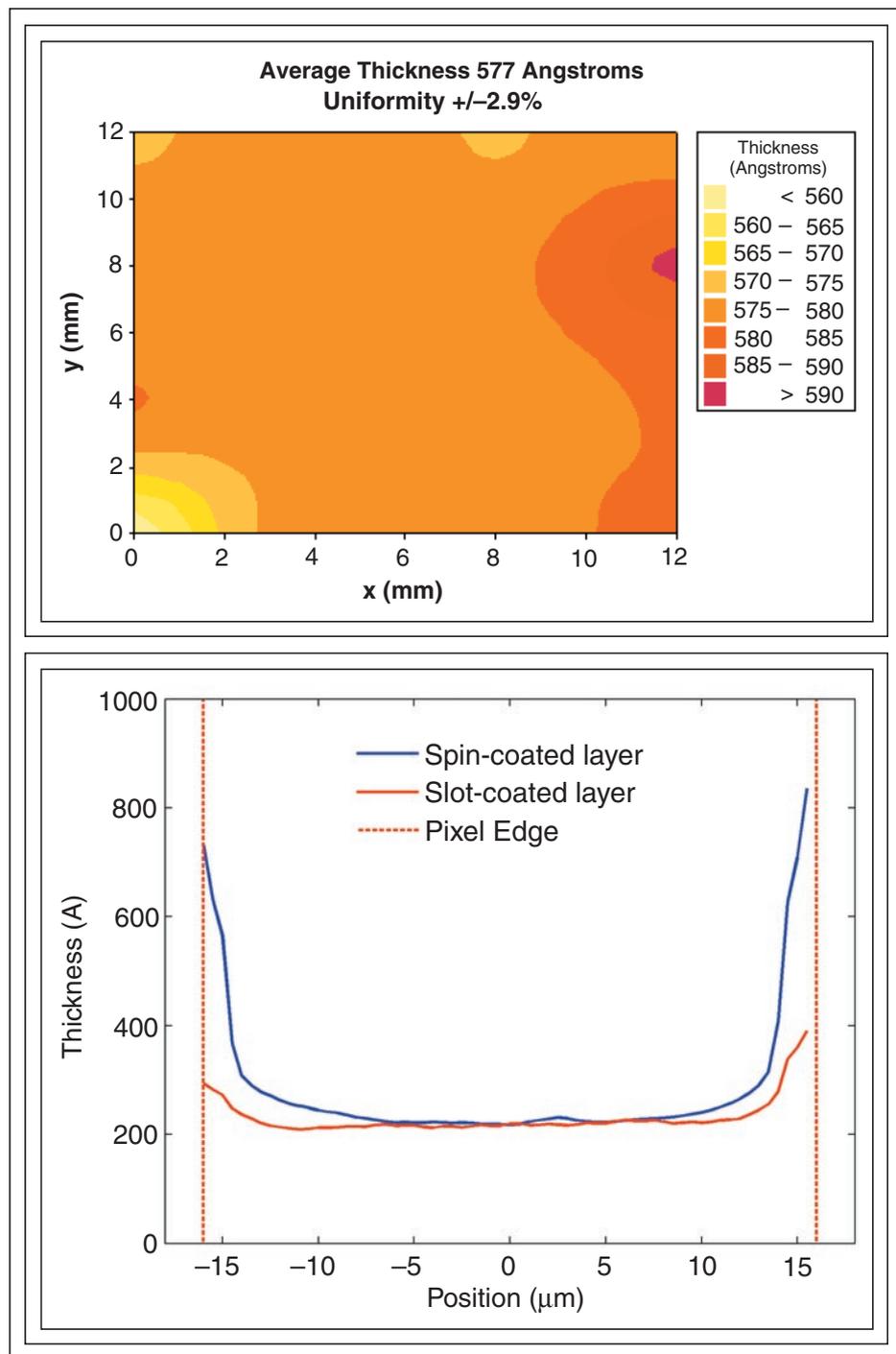
Continuous nozzle printing utilizes a laminar liquid jet that issues from a fixed orifice and then impinges on the substrate. The printing process operates by continuously moving the liquid jet across the substrate in alignment with previously defined wetting and non-wetting areas. The printhead traverses back and forth along the x-axis of the printed plate while the stage (substrate) proceeds in increments along the y-axis in synchronization with the head. Commercially acceptable cycle times can be obtained by printing multiple arrays of jets using x-axis traverse speeds

Slot-Die Coating is the preferred commercial solution-coating technique for preparing thin uniform blanket layers, and this technique has been scaled up to (at least) Gen 8 substrates for flat-panel-display processing. Slot-die coating is also being developed for use in general-lighting-based OLED applications.[4] Figure 3 (top) shows optical profilometer data plotted as a contour map of our company's HIL slot-die coated onto a 150 × 150-mm glass substrate. In this sample layer, we achieved, via slot coating, better than ±3% long-range layer thickness uniformity for a layer as thin as 600 Å.[a]

Through optimization of formulation, die geometry, coating, and drying, we found that slot-die coating can deposit 2–10-μm-thick wet layers over relatively tall (~1 μm) display topography such as bus lines, pixel-defining layers, and circuit vias. However, differences in wetting due to surface material type (for example, ITO *vs.* photoresist) and surface-tension gradients can cause thickness non-uniformity in the dried film that must be minimized. We define thickness aperture, a figure of merit for characterizing intra-pixel thickness uniformity, as the percentage of pixel cross-section within ±10% of the center of pixel thickness (nominal target thickness). Figure 3 shows a comparison of spun *vs.* slot-die coated subpixel HIL layer thickness, for a 225-Å target thickness. The slot-die coated layer has a much higher thickness aperture at

Fig. 2: At left is an architectural cross-section of a solution-processed OLED device. The middle shows a schematic cross-section of high and low intra-pixel uniformity in OLED layers (not to scale) and at right is a corresponding example of blue-subpixel EL images.

up to 5 m/sec.[6] Nozzle printers suitable for printing solution layers for large-scale AMOLED displays have been developed together with Dainippon Screen Mfg. Co., Ltd. (Kyoto, Japan) and a multi-nozzle printer capable of Gen 4 (refers to stage size) substrates has been installed at DuPont Displays' pilot facility in Santa Barbara, California.

The key elements of nozzle printing are

- Establishing a stable laminar jet.
- Scanning the jet across the substrate.
  - During this time, the ink spreads on the substrate due to inertia and retracts back to the wetting region of the previously formed containment pattern.
- Advancing the substrate while the nozzle is off the printed region.
- Drying to a uniform thickness profile.

Several approaches for forming a containment pattern suitable for printing OLED displays are described in the literature. DuPont Displays' proprietary ink-containment pattern (Fig. 2) is created during the OLED-fabrication process and requires no physical containment structures. The containment process forms wetting and non-wetting regions on the substrate to help contain the red, green, and blue EML inks; the main purpose of containment being to prevent cross-contamination between the inks.

While the length over which the liquid jet is stable determines the lower limit for flow rate, the upper limit is set by the orifice (nozzle) opening and the gap between the orifice and substrate. Laminar jet stability has been studied extensively, and these studies have explored the effects of jetting parameters (orifice size, fluid velocity, and motion of the surrounding gas) and liquid properties (surface tension, viscosity, changing composition, and viscoelasticity).[7]

We captured high-resolution high-magnification images of our printing jets and measured the stable length. For long stable jet lengths, the predictions of a literature model[8] are in reasonable agreement with our observations. However, the model severely overpredicts the lower limits of stable jet length. We used a value of the initial jet perturbation $\eta_{0/a} \sim 0.07\%$ in the Mahoney-Sterling model, which is typical in the literature. Experimentally, we found that the disagreement with the model is due to distortion of the jet as it begins to wet the nozzle face. Upon impact, the jet spreads due to inertial forces. Obviously, spreading must be controlled to prevent color contamination, *e.g.*, printing green ink into a blue subpixel. The need to control spreading generally determines the upper limit on ink flow rate.

Fig. 3: *At top is a thickness contour map of an HIL slot coated on a 150 × 150-mm bare glass substrate; the coating has a uniformity of ±2.9% of the 577-Å layer. At bottom is shown a stylus profilometer measurement of a subpixel (cross-section), comparing spin vs. slot-coated layer thickness within a subpixel.*

We performed computational fluid-dynamic (CFD) modeling to better understand inertial spreading in nozzle printing. All CFD modeling used FLOW-3D, a volume of fluid simulation package from Flow Science, Inc., located in Santa Fe, New Mexico (www.flow3d.com). Figure 4 shows a sample CFD simulation output of axisymmetric impingement of a laminar jet on a surface. To verify the model's ability to predict inertial spreading, we simulated hydraulic jumps, which have previously been well-described and pictured at larger length scales.[9] We found no literature data for hydraulic jumps at lengths typical of our printing process, so we obtained jump radii (R_h) using the setup shown in Fig. 4. We obtained good agreement between CFD simulations and our experimental results.

Figure 4 (lower) shows a CFD simulation of a simple printing flow. The jet moves across a substrate with a surface-tension pattern that prevents overflow to neighboring print lanes. The top-view image (middle) shows the wet line deposited as the jet passes. The dashed red lines represent the boundary of the wetting region, with a non-wetting surface outside the boundary. Initially, the liquid spreads onto the repellent surface due to inertia and retracts back to the containment boundaries as surface tension establishes an equilibrium meniscus shape. The graphic on the right shows a time series of the line profile, starting at the point of widest spreading and progressing toward the final equilibrium shape.

Customized metrology and analytical methods have been developed in our laboratories for measuring thickness and luminance uniformity in our solution-coated AMOLED displays. Excellent intra- and inter-pixel and long-range thickness uniformity is required across several orders of magnitude in length scale, from tens of microns to tens of centimeters or larger. As a result, we have developed multiple techniques to study and optimize the uniformity of the liquid deposition and drying processes.

The presence of pixel wells complicates drying by distorting the meniscus. Careful control of the drying rate, surface tension, and viscosity are important factors for achieving uniform films. We constructed a drying model to help us understand and optimize the drying process. Practical inks often contain multiple solvents, and mixture evaporation is best described using non-ideal vapor pressures. We estimate the activity coefficients
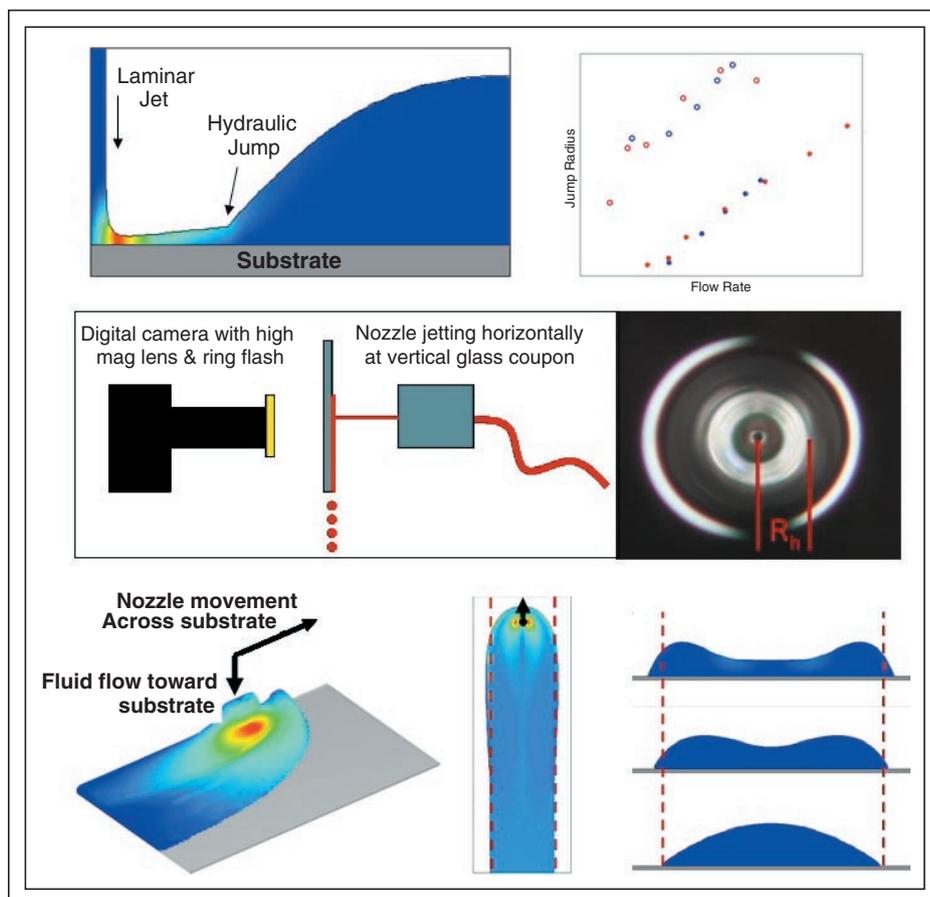
Fig. 4: At upper left, a CFD simulation of axisymmetric impingement of a laminar jet on a surface is depicted. At the hydraulic jump, the fluid slows and the liquid-layer height increases significantly. Color (blue to red) indicates magnitude of radial velocity (low to high). At right is shown the hydraulic jump radius for two nozzles plotted vs. flow rate. Blue symbols represent experimental data and red symbols represent CFD simulation. The upper set of results has been offset vertically for clarity. At middle is a schematic of the hydraulic jump measurement apparatus and a sample image used to measure R_h. At lower left is a perspective view of CFD simulations of a simple printing flow. The jet moves across a substrate with a surface-tension pattern that prevents overflow to neighboring print lanes. The hydraulic jump is distorted by the movement of the nozzle across the surface. Colors indicate the magnitude of the lateral fluid velocity. Lower-middle is the top view: the wet line is deposited as the jet passes. The dashed red lines represent the boundary of the wetting/non-wetting region. Lower right: substrate plane view. A time sequence shows liquid spreading onto the non-wetting surface due to inertia and retracting to an equilibrium shape on the wetting pattern.

for the ink solvents using the UNIFAC (Universal Functional Activity Coefficient) group contribution method.[10] Using an adaptive time step model, with correlations fit to surface tension and viscosity data, allows us to predict the evolution of fluid properties through the drying process in order to control the resultant film shape and optimize for flat films.

To characterize the intra-pixel and long-range uniformity of a printed layer, we used a standard stylus profilometer to measure multiple spots on the printed display. In this technique, we left an unprinted pixel row with identical underlayers next to the printed pixel row. We then subtracted the underlying layers from the unprinted row to get a measure of the film thickness as a function of

position within the pixel. Automated software was developed to analyze large data sets across various display designs and resolutions. Figure 5 (left) shows thickness profiles for EML films with good uniformity measured at 16 locations across a 150×150-mm printed substrate. This data set has a standard deviation of 2 nm, with a 38-nm center-of-well thickness resulting in $\pm5\%$ long-range uniformity, illustrating the high level of long-range uniformity in our printing process. A thickness aperture metric, similar to that described for slot-coated layers, helps to numerically describe the intra-pixel uniformity; typically a >95% thickness aperture is achievable for pixels suitable for AMOLED TVs. This custom measurement system provides direct and immediate feedback for process development without requiring the fabrication of full OLED devices. Consequently, we are able to quickly tune our ink formulation and process conditions in order to optimize intra-pixel and long-range uniformity.

In combination with measuring the intra-pixel thickness uniformity of the slot-die-coated and nozzle-printed layers, we can also measure the uniformity of light emission from the pixels in a completed device. Here, we use a microscope camera to obtain high-resolution images of discrete pixels. We then use custom image-analysis software to measure the luminance intensity across the pixel. This technique yields profiles that are analogous to the film-thickness profiles described previously; an example is shown in Fig. 5 (right). It is

particularly useful to correlate the thickness profiles for the solution-processed layers with the luminance-uniformity measured from the completed OLED to improve performance.

It is well known that jetting simultaneously out of multiple orifices presents a challenge for printing technologies, due to short-range luminance variation that can occur between subpixels of the same color, sometimes called stitching or swath marks.[11] The authors previously described this problem for nozzle printers, as well as several implemented fixes in a 2009 SID Symposium presentation, "Multi-Nozzle Printing: A Cost-Effective Process for OLED Display Fabrication."[6] In nozzle printing technology, each nozzle acts as an independent flow element with separate mass-flow controllers, so it is very important that nozzle flows match in order to produce films of identical thickness in neighboring subpixels. As a consequence, we developed techniques to characterize the uniformity from subpixel to subpixel.

To compare the deposited volume of ink between two or more nozzles, we used an optical profilometer to obtain images of printed lines on smooth glass substrates. We then computed the volume of each line, using software we developed for this purpose. Next, this method was calibrated using measurements made on a plate where flows had been intentionally offset between two nozzles. We have confidence that this technique is capable of studying differences in deposited volumes of less than 1%.

Short-range luminance uniformity (SRU) is a complicated display metric due to the variety of resolutions, viewing environments, and human physiological responses. A well-defined automated machine-vision inspection metric has yet to be defined. To examine the effect of coating uniformity, and, in particular, printing-layer inter-pixel uniformity in our AMOLED displays, we used an SRU specification that had previously been reported to compare commercial AMLCD and AMOLED technology.[12]

We obtained a map of the luminous intensity of each subpixel using a linear high-resolution CCD camera in conjunction with a video-photometer and custom image-analysis software. We then used formulae[13] that determine the ratio for the maximum and minimum luminance to calculate the SRU of each subpixel and neighbors in an 8×8 block. We repeated the analysis for each subpixel in the display to generate SRU maps as shown in Fig. 6. The overall SRU for the display is an average of all the block SRU values.[14] A commercial AMLCD measured by this method had an SRU of 0.93. DuPont solution-processed AMOLED displays have equal or greater SRU values for each color, thus demonstrating the high uniformity of this solution-coating technology.

Our OLED materials have demonstrated superior performance. Table 1 shows printed OLED device performance of current generation materials using a common thickness for all layers except the EML.[15] All printed device data are collected from devices fabricated in an ambient atmosphere clean-room environment, using the same types of processing techniques planned for commercial manufacturing of solution-processed OLED displays.

In order to prove performance, DuPont Displays fabricated multiple solution-coated AMOLED displays for the SID's Display Week 2010 exhibition. Figure 7 shows front- and side-view images of a 4×4 array representing a segment of a 40-in. HDTV. The 16 AMOLED displays used in this demonstration were fabricated similarly to the one for which luminance SRU was measured (Fig. 6).

This solution AMOLED technology can be leveraged into other solution-based organic-semiconductor applications such as OLED lighting and organic solar cells. Specifically, we are extending the materials, processing, and architecture know-how generated in
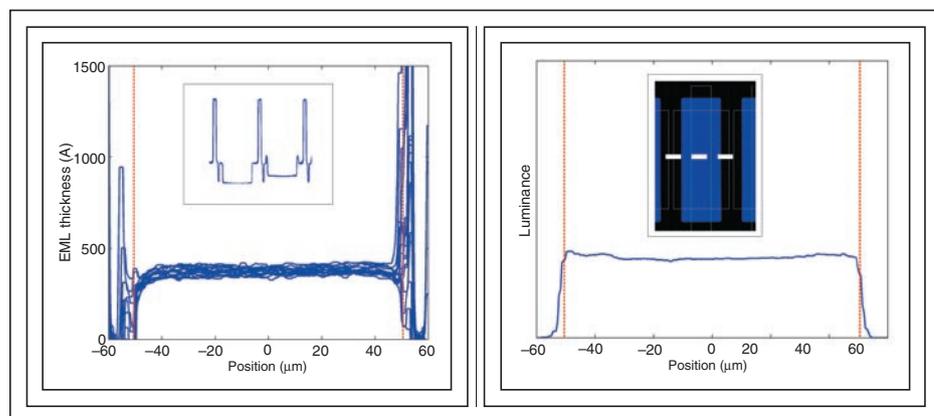
Fig. 5: *At left are printed film profiles obtained with a stylus profilometer and a custom automated software analysis program. The inset shows a sample of the raw scan data where a printed row is located next to an unprinted row with identical underlayers. The red dashed lines represent the edge of the pixel. On the right is an example of a luminance intensity plot used to analyze intra-pixel uniformity.*
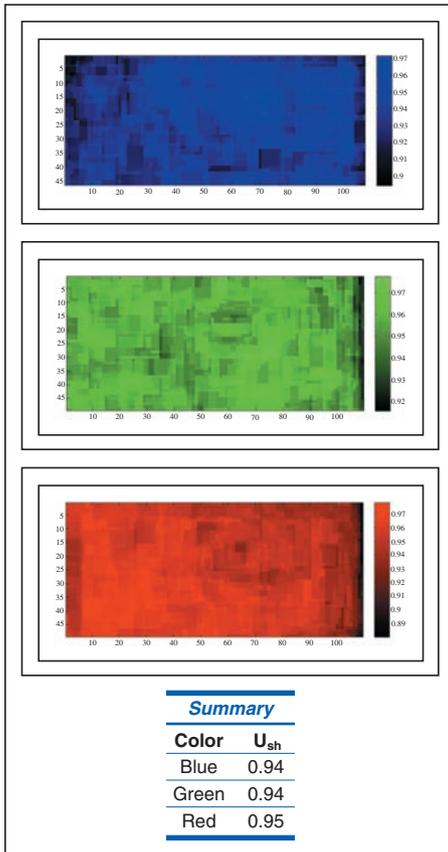
Summary	
Color	**U_{sh}**
Blue	0.94
Green	0.94
Red	0.95

Fig. 6: Shown is a uniformity map of SRU (UR_{ij}) over a large section of a printed AMOLED display and the average SRU (U_{sh}) for each color (table). These SRU values equal or exceed the values reported for commercial AMLCDs.[12]

Table 1: This printed RGB test coupon performance summary uses a T50 adjusted OLED-TV lifetime (conservatively estimated using all pixels on, 100% of the time) and measured efficiency for simulated OLED-TV conditions.[16]

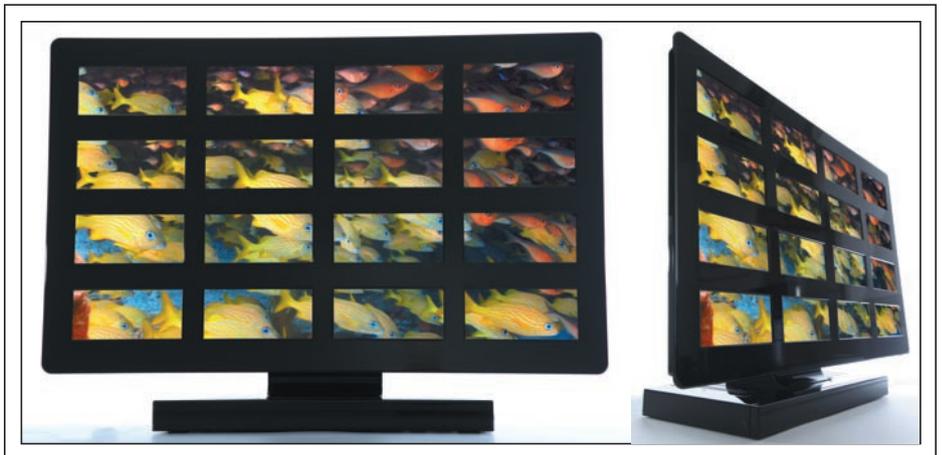| Color	CIE 1931 x,y	Efficiency (cd/A)	Printed T50 lifetime (hours)
Red	0.65, 0.35	15.1	29,000
Green	0.26, 0.64	21.9	230,000
Blue	0.14, 0.14	6.0	40,000

Fig. 7: This prototype AMOLED-TV array was made with DuPont's OLED solution-processing technology and materials and was exhibited at the Society for Information Display's Display Week 2010. The array is composed of 16 4.4-in.-diagonal 55-ppi displays, representing a segment of a 40-in. HDTV.

AMOLED to color-tunable white lighting under a Department of Energy Solid State Lighting Project titled "Solution-Processed Small-Molecule OLED Luminaire for Interior Illumination." The white-lighting project aims for 40 lm/W using separate printed yellow, orange, and blue emitter layers, which allow color tuning of the luminaire white point.

Summary

DuPont Displays has developed a full set of high-performance materials and solution-processing technology to address the high cost of manufacturing AMOLEDs. We optimized our coating processes to be cost and performance competitive with existing commercial vapor-deposition technology. The brightness and color-uniformity specifications for flat-panel displays present challenging thickness and uniformity requirements for solution-coated AMOLED layers. Using a wide variety of custom modeling and analytical approaches, we have developed short- and long-range film-thickness control and uniformity that is commercially viable at large glass sizes. These coating technology improvements should extend to other solution-based applications as well.

References

[a]Formula for uniformity =
$$\pm[(T_{max} - T_{min})/(T_{max} + T_{min})].$$
[1]A. C. Arias *et al.*, "Materials and Applications for Large-Area Electronics: Solution-Based Approaches," *Chem. Rev.* **110**, 3–24 (2010).
[2]W. F. Feehery *et al.*, "Solution Processing for OLED Industry Success," *Information Display* **23**, 28–33 (2007).
[3]W. F. Feehery, "Turning Solution Processed OLED Displays into Reality," SID 2008 Business Conference.
[4]T. Kawaguchi *et al.*, "Visualization technique for slit coat method," *Proc. IDW '09,* 1037–1040 (2009).
[5]T. J. Faircloth, J. G. Innocenzo, and C. D. Lang, "Slot Die Coating for OLED Displays," *SID Symposium Digest* **29**, 645–647 (2008).
[6]R. J. Chesterfield *et al.*, "Multinozzle Printing: A Cost-Effective Process for OLED Display Fabrication," *SID Symposium Digest* **30**, 951–954 (2009).
[7]H. C. Burkholder and J. C. Berg, "Effect of Mass Transfer on Laminar Jet Breakup," *AICHE J.* **20**, 863-872 (1974).
[8]T. J. Mahoney and A. M. Sterling, "The Breakup Length of Laminar Newtonian Liquid Jets in Air," *Proceedings of the First International Conference on Liquid Atomization & Spray Systems* (1978).
[9]S. Middleman, *Modeling Axisymmetric Flows: Dynamics of Films, Jets, and Drops* (Academic Press, New York, 1995), Ch. 5.

[10]A. Fredenslund, J. Gmehling, and P. Rasmussen, *Vapor-Liquid Equilibrium Using UNIFAC* (Elsevier, 1977).

[11]J. Lee, "Technical Challenges for Polymer OLED Manufacturing," *IMID Symposium Digest*, 1165 (2008).

[12]A. Arkhipov, B-W. Lee, K. Park, C. Kim, and J. Lee, "New Metric for Short-Range Uniformity of AMOLEDs," *IMID Symposium Digest*, 488-491 (2008).

[13]$Ush = \dfrac{\sum_{i=0}^{n-1}\sum_{j=0}^{m-1} Ur_{ij}}{n \times m}$ where $Ur_{ij} = 1 - \dfrac{L_{64\max} - L_{64\min}}{L_{64\max}}$,

$L_{64\max} = \max_{i=0...7, j=0...7} L_{ij}$, $L_{64\min} = \min_{i=0...7, j=0...7} L_{ij}$

[14]Shorted pixels and dead pixels were omitted for this analysis.

[15]R. Pflanzer, *IMID Symposium Digest* (2010).

[16]No outcoupling enhancement efficiency. Measurement assumes Lambertian emission profile. Common architecture converted to 200 nits front-of-screen (white point CIE x,y = 0.31, 0.32) with 40% aperture ratio, 46% transmission circular polarizer, driven at a 100% duty cycle. Lifetime data reported at 20°C. ∎